Thermochemical studies of reactions of Re^+ with SO_2 using guided ion beam experiments and theory†

JungSoo Kim, Richard M Cox,‡ and P. B. Armentrout*

Department of Chemistry, University of Utah, 315 S 1400 E Rm 2020, Salt Lake City, UT 84112

The kinetic energy dependent reactions of Re^+ with SO_2 were studied with guided ion beam tandem mass spectrometry. ReO^+, ReO_2^+, and $OReS^+$ species were observed as products, all in endothermic reactions. Modeling of the kinetic energy dependent cross sections yields 0 K bond dissociation energies (BDEs, in eV) of 4.78 ± 0.06 (Re^+-O), 5.75 ± 0.02 (Re^+-O_2), and 4.35 ± 0.14 (Re^+-SO). The latter two values can be combined with other information to derive the additional values 6.05 ± 0.05 (ORe^+-O) and 4.89 ± 0.19 (ORe^+-S). BDEs of ReO^+ and ReO_2^+ agree with literature values whereas the values for $OReS^+$ are the first measurements. The former result is obtained even though formation of ground state ReO^+ is spin-forbidden. Quantum mechanical calculations at the B3LYP level of theory with a def2-TZVPPD basis set yield results that agree reasonably well with experimental values. Additional calculations at the BP86 and CCSD(T) levels of theory using def2-QZVPPD and aug-cc-pVxZ (x = T, Q, and 5) basis sets were performed to compare thermochemistry with experiment to determine that ReO_2^+ rather than the isobaric ReS^+ is formed. Product ground states are $^3\Delta_3$ (ReO^+), $^3B_1$ ($OReO^+$), $^5\Pi_{-1}$ (ReS^+), and $^3A''$ ($OReS^+$) after including empirical spin-orbit corrections, which means that formation of ground state products is spin-forbidden for all three product channels. The potential energy surfaces for the $ReSO_2^+$ system were also explored at the B3LYP/def2-TZVPPD level and exhibited no barriers in excess of the endothermicities for all products. BDEs for rhenium oxide and sulfide diatomics and triatomics are compared and discussed. The present result for formation of ReO^+ is compared to that for formation of ReO^+ in the reactions of Re^+ + O_2 and CO, where the former system exhibited interesting dual cross sections features. Results are consistent with the hypothesis that the distinction of in-plane and out-of-plane C_S symmetry in the triatomic systems might be the explanation for the two endothermic features observed in the Re^+ + O_2 reaction.

‡ Present address: Pacific Northwest National Laboratory, 902 Battelle Blvd., Richland, WA 99352

† Electronic supplementary information (ESI) available: Table S1 lists vibrational frequency scaling factors used. Tables S2 and S3 provide molecular constants and energies calculated at several levels of theory for SO_2 and ReS^+, respectively. Table S4 lists geometrical information and energies for various species along the $ReSO_2^+$ reaction surface. See DOI: 10.1039/c9cpxxx

ORCID: P. B. Armentrout: 0000-0003-2953-6039

Introduction

Our laboratory has recently studied the reactions of several late third-row transition metal cations (M^+ = Re^+, Os^+, and Ir^+) with O_2 by guided ion beam tandem mass spectrometry, thereby elucidating the kinetic energy behavior in the formation of the MO^+ product ion.[1-3] In all three cases, the cross sections of the $MO^+ + O$ products exhibited two endothermic features as the kinetic energy was varied. The origins of this relatively unusual behavior were explored with several possible explanations proposed. These included reactions of excited states, the possibility of conservation of spin or lack thereof between the electronic states of the reactants and the products, and the possibility of both in-plane (A′) and out-of-plane (A″) symmetries of the intermediates. The presence of excited state reactants could be ruled out experimentally. Spin conservation is difficult to rationalize because both the O_2 reactant and O product have triplet spin, which means that a multitude of spin states of M^+ and MO^+ can be coupled while still conserving spin. A′ and A″ symmetry occurs in these systems because the reactions involve only three atoms, such that there is always a plane of symmetry (C_s).

To further probe the possible explanations, additional experiments of the same three metal cations were performed with CO.[4] In these systems, the triatomic character of the reactions is retained, but now the neutral reactant has a singlet state, which limits which states of MO^+ can be formed along spin-allowed pathways. In these studies, the cross sections of the $MO^+ + C$ (^3P) products exhibited only one endothermic feature; however, this could be a consequence of the much higher bond dissociation energy (BDE) of CO (11.111 eV) compared to that for O_2 (5.117

eV).[5]

The current study is intended to further elucidate the origins of the interesting kinetic behavior observed in the $M^+ + O_2$ reactions. Here, reaction of Re^+ with SO_2 is studied as a function of kinetic energy. SO_2 has a singlet spin ground state and SO has a triplet ground state, such that the spin restrictions associated with forming ReO^+ are the same as for the reaction of Re^+ with CO. However, the plane of symmetry constraining the reactions of M^+ with diatomic O_2 and CO is removed because the $ReSO_2^+$ intermediates are composed of four atoms. Further, D_0(O-SO) = 5.66 eV[5] is similar to $D_0(O_2)$, such that thermodynamic differences in the behavior should be minimized. In addition, information is also obtained on competing reactions, which include the formation of ReO_2^+ and $ReSO^+$. Thermochemistry for all products are determined by analyzing their kinetic energy dependent cross sections. Further, the reaction products and mechanisms for their formation are explored computationally.

Experimental and Computational Section

Experimental Details

The guided ion beam tandem mass spectrometer (GIBMS) with which this work was performed has been described in detail previously.[6] Briefly, a direct current discharge and flow tube (DC/FT) ion source was utilized.[7] In this source, a strong electric field (1.2 – 1.5 kV) ionized Ar, which sputtered the rhenium sample comprising the cathode to generate the Re^+ reactant ions. These ions entered the flow tube along with the carrier gas (90%/10% He/Ar) at ~0.4 Torr, where they underwent ~10^5 thermalizing collisions. The distribution of electronic states of these reactant ions in the DC/FT source have been characterized by effective temperatures of 300 – 1100 K.[8-13] Over this temperature range, 100% pure ground level Re^+ ($^7S_3$) was created. In previous studies of the reactions of Re^+ with O_2, CO, H_2, and CH_4 using the same ion source, there was no evidence for excited states,[1, 4, 14-15] in agreement with results of the current study.

The ions were extracted from the flow tube and then focused into the magnetic sector momentum analyzer for mass selection of the reactant ions. These reactant ions were decelerated

to well-known kinetic energies and focused into an octopole ion guide where the ions were radially constrained by radio frequency (rf) electric fields.[16-18] The octopole passed through a static reaction cell where the reactant neutral (SO_2) was introduced at pressures ranging from 0.1 to 0.4 mTorr. These low pressures significantly decrease the possibility of multiple collisions. Nevertheless, there is evidence of pressure dependent cross sections for certain products. Rigorous single collision cross sections were regained by extrapolating the results to zero pressure of SO_2. After passing through the octopole, ions were extracted, refocused into a quadrupole mass filter for mass analysis, and detected with a Daly detector.[19] Absolute reaction cross sections were calculated as described previously from product ion intensities relative to the total ion intensity after correcting for background signals obtained with no SO_2 in the reaction cell.[18] Uncertainties in the absolute cross sections were estimated as ±20% and relative uncertainties as 5%. Laboratory frame energies were converted to center-of-mass (CM) frame energies using $E_{CM} = E_{lab} \times m/(m + M)$, where m and M are the masses of neutral and ionic reactants, respectively. Cross sections are broadened by several effects including the kinetic energy distribution of reactant ions and the thermal motion of reactant neutrals (Doppler broadening).[20-21] As described previously,[18] the octopole ion guide was used as a retarding analyzer to determine the full width at half maximum (fwhm) of the kinetic energy distribution of the reactant ions and the absolute zero of the kinetic energy. The fwhm of the kinetic energy distributions in this study was between 0.49 and 0.55 eV (Lab). The uncertainty in the energy scale is ±0.05 eV (Lab).

Data Analysis

Endothermic reaction cross sections in this study were modeled using the modified line-of-centers (MLOC) model shown in eq (1),

$$\sigma(E) = \sigma_0 \Sigma g_i (E + E_{el} + E_i - E_0)^n/E \qquad (1)$$

where σ_0 is an empirical scaling parameter, E is the center-of-mass frame energy, E_{el} is the average electronic energy of the metal ion (0.000 eV for Re^+), E_i is the internal energy of the neutral reactant having rovibrational states i with population g_i ($\Sigma g_i = 1$) at the reaction cell temperature

of 305 K, E_0 is the threshold energy at 0 K, and n is an empirical fitting parameter. Before comparison with the experimental data, this model was convoluted over the kinetic energy distributions of the reactants.[18, 21] Then, the parameters, σ_0, E_0, and n were optimized by a nonlinear least-square method for best reproduction of the experimental reaction cross sections. Uncertainties in the modeling parameters were obtained via analyses of several data sets using a range of acceptable n values and includes the absolute uncertainty in the CM energy scale.

At energies above D_0(O-SO) and D_0(S-O_2), product ions can dissociate. This behavior was modeled by including P_D, the probability of product ion dissociation in the model, as described previously.[22] Two parameters, p, similar to n but limited to integral values, and E_D, the energy where the product ion begins to dissociate, control P_D. These two parameters were optimized for best reproduction of experimental data at high-energies but did not affect the threshold determinations.

All products observed in the reaction of Re^+ with SO_2 are believed to share a common intermediate, ORe^+OS, such that these products can compete with each other. Such competition is evidenced by product cross sections peaking at the onset for new product channels rather than where the product can dissociate, which correlates with BDEs of the reactant neutral. To reproduce the behavior of these competing product channels, a phase space theory (PST) competitive model that explicitly conserves angular momentum was used, as detailed elsewhere.[23-25] Input parameters needed for the PST model include molecular constants of the reactants and products, which were taken from theory (see below), and the E_0 threshold energy for each channel, which were allowed to vary to best reproduce the data. We also permitted the number of accessible surfaces to vary to reproduce the magnitudes of the competing cross sections. Finally, the absolute magnitude of the PST model is ordinarily limited by the Langevin-Gioumousis-Stevenson (LGS) model for collisions between ions and molecules.[26] However, this model drops below the hard sphere (HS) collision cross section, estimated to be 4.0×10^{-15} cm^2 on the basis of the radii of the reactants, at energies above about 1 eV. Therefore, the collision cross section (LGS below 1 eV, HS above) was multiplied by the branching ratio calculated by PST to reproduce the experimental cross

sections over a wider range of collision energies. As angular momentum is not rigorously conserved for HS collisions at the higher energies, this could lead to some discrepancies with experimental results.

The threshold energies, E_0, obtained from the modeling either with MLOC or PST can be converted to BDEs of the observed products using eqs (2) or (3),

$$D_0(Re^+\text{-}L) = D_0(O\text{-}SO) - E_0 \qquad \text{for L = O and SO} \qquad (2)$$

$$D_0(Re^+\text{-}L) = D_0(S\text{-}O_2) - E_0 \qquad \text{for L = S or } O_2 \qquad (3)$$

where $D_0(O\text{-}SO) = 5.66 \pm 0.02$ eV and $D_0(S\text{-}O_2) = 5.900 \pm 0.004$ eV.[5] Eqs (2) and (3) assume that there is no activation barrier in excess of the endothermicity for the reaction of interest. This assumption is usually appropriate because of the long-range attractive force between ions and molecules.,[18, 27-28] The present theoretical results indicate this assumption also applies in the present work.

Theoretical Calculations

Quantum chemistry calculations in the current study were performed with the Gaussian09 suite of programs.[29] Previous studies of similar systems suggest that B3LYP hybrid density functional theory[30-31] and CCSD(T)[32-35] provide thermochemistry in reasonable agreement with experimental BDEs.[1-4, 15, 36-37] The CCSD(T) approach was used for single point energy calculations using B3LYP optimized structures and zero-point corrections. Basis sets used included def2-XZVPPD (X = T and Q) and aug-cc-pVXZ (X = T, Q, and 5)[38-40] which were imported from the EMSL basis set exchange.[41-42] For the metals, these basis sets use effective core potentials (ECPs) that are small core (60 electrons) with explicit 5s, 5p, 5d, and 6s valence orbitals. Additionally, complete basis set (CBS) extrapolations were performed using the method of Halkier et al., which uses two point (Q, 5) protocols for both Hartree-Fock energies and CCSD(T) correlation energies.[43-46]

All theoretical frequencies and zero-point energies were scaled with the scaling factors listed in Table S1 (ESI†). These scaling factors were either taken directly from Kesharwani et al.[47] or were determined from similar levels of theory and basis set combinations. Calculated bond

energies of SO_2 are in reasonable agreement with experiment [5] at all levels of theory, as shown in Table S2 (ESI†), generally lying within 10% (although this corresponds to discrepancies as high as ~0.6 eV). BP86 and CCSD(T) approaches generally give results within 5% (discrepancies <0.3 eV). Vibrational frequencies and rotational constants of SO_2 are also reproduced well at nearly all levels used, Tables 1 and S2 (ESI†).

Experimental Results

Reactions of Re^+ with SO_2

Figure 1 shows the products formed in reactions of Re^+ with SO_2. The main products observed correspond to reactions (4) – (6), all of which clearly exhibit thresholds and none of which exhibit any dependence on the SO_2 pressure.

$$Re^+ (^7S_3) + SO_2 (^1A_1) \rightarrow ReO^+ + SO \quad (4)$$

$$\rightarrow ReO_2^+ + S \quad (5a)$$

$$\rightarrow ReS^+ + O_2 \quad (5b)$$

$$\rightarrow ReSO^+ + O \quad (6)$$

Note that reaction (5) can be assigned to two isobaric possibilities. In addition, both $ReSO_2^+$ and $ReSO_3^+$ are formed in barrierless exothermic reactions at low energy. The cross sections for both $ReSO_2^+$ and $ReSO_3^+$ are linearly dependent on SO_2 pressure, consistent with their formation in two collisions with SO_2. These products disappear after extrapolation to zero SO_2 pressure. It can be seen that the cross section for ReO_2^+ (plausibly ReS^+) begins at low energies and then rapidly reaches a maximum at the onset of production of ReO^+. This cannot be because the ReO_2^+ product dissociates to form ReO^+, as the formation of $ReO^+ + S + O$ requires substantially more energy (as detailed below). Rather, this indicates that these two products must share a common intermediate and therefore compete with one another. This is confirmed by the calculations of the potential energy surfaces (PESs) for these reactions below, which also indicates that the $ReSO^+$ product channel similarly competes with the other two major product channels. At still higher energies, the products may have sufficient energy to dissociate, and therefore the product cross sections begin

to decline more rapidly. For ReO^+ and $ReSO^+$, this can occur starting at D_0(OS-O) = 5.66 eV, and for ReO_2^+ and ReS^+, dissociation can begin at D_0(S-O_2) = 5.90 eV.[5] Cross sections for the latter two products exhibit fast declines beginning at these energies, Figure 1, whereas that for ReO^+ shows a much slower decline. These results suggest that the diatomic SO product accompanying ReO^+ in reaction (4) carries away significant amounts of energy compared to the atomic neutral products of reactions (5a) and (6).

PST modeling of reaction cross sections

As noted above, the three main channels observed in the reactions of Re^+ with SO_2 display behavior as a function of energy consistent with competition among these channels. In order to model this competition, the PST model was used to analyze the data as shown in Figure 2. Parameters used in the model are listed in Table 1 with the only adjustable parameters being the E_0 threshold energy for each channel and the number of accessible surfaces. It can be seen that the PST model reasonably reproduces the competitive behavior of all three channels up to about 3 eV and accounts for the peak in the ReO_2^+/ReS^+ cross section, although the detailed behavior of the ReO_2^+/ReS^+ channel at its peak is not modeled with fidelity.

MLOC modeling of reaction cross sections

Close inspection of Figure 2 illustrates that the PST model does not reproduce the threshold regions of any of the channels with complete accuracy. This is likely to be a consequence of trying to reproduce the cross sections over such an extended energy range. To test this, the cross sections were also modeled using the modified line-of-centers (MLOC) model, eq (1), in the threshold regions, as shown in Figure 3. For the lowest energy channel, complications associated with competition were avoided by modeling the total cross section instead of the individual cross section for ReO_2^+/ReS^+. Optimized parameters for eq (1) are provided in Table 2.

With the MLOC model, the ReO^+ and total cross sections are reproduced well up to ~2.5 eV with reasonable n values of 2.2 ± 0.1. The $ReSO^+$ cross section is reproduced well up to over

8 eV using a reasonable *n* value and addition of product dissociation (P_D) above D_0(OS-O). The threshold energies for the PST and MLOC models are similar to one another (within 0.18 eV). Further evaluation of which approach provides the most accurate thermochemistry can be made by comparison with literature bond energies, as discussed below.

ReO^+ thermochemistry

Thermochemistry for the ReO^+ species has been discussed in detail previously.[1, 4] Prior to our guided ion beam (GIB) studies, the literature thermochemistry for ReO^+ was sparse (as reviewed previously),[1] with the best value coming from crude CID experiments of Bondybey and co-workers, $D_0(Re^+\text{-}O) = 5.0 \pm 1.3$ eV.[48] Our GIB studies of the reactions of Re^+ with O_2 and CO provided consistent but much more precise measurements, with the O_2 system having a lower uncertainty. These values are all listed in Table 3.

By using eq (2) and the MLOC threshold of ReO^+ listed in Table 2 (0.88 ± 0.05 eV), a BDE of Re^+-O is obtained as 4.78 ± 0.06 eV. As shown in Table 3, this value agrees well with previous GIB values. In particular, it lies within experimental uncertainty of the measurement of $D_0(Re^+\text{-}O)$ from the $Re^+ + O_2$ GIB experiment,[1] which represents our best available value, in part because there are no competing reactions in this system.

Alternative analyses of these data using the PST model yield a threshold of 1.00 ± 0.04 eV for ReO^+, which leads to a BDE of 4.66 ± 0.06 eV. This BDE is in reasonable agreement with the literature thermochemistry, but with a deviation from the value obtained in the GIB O_2 experiment of 0.16 ± 0.07 eV, compared with a value within uncertainty obtained from the MLOC analysis. Thus, we believe that the MLOC analysis provides more accurate thermodynamic information compared to the PST model, because the latter is sufficiently constrained by the simultaneous analyses of all product cross sections that it cannot reproduce the onsets of the product cross sections precisely, compare Figures 2 and 3. However, the PST model does provide a better overview of the cross section behavior over longer energy ranges, including the competition among the three reaction channels.

ReO_2^+/ReS^+ thermochemistry

As introduced above, the ReO_2^+/ReS^+ product is formed in reaction (5). Using the MLOC threshold in Table 2 (0.15 ± 0.02 eV), eq (3) leads to a BDE value for $D_0(Re^+\text{-}O_2)$ or $D_0(Re^+\text{-}S)$ of 5.75 ± 0.02 eV. This value agrees with a previous literature value of 7.1 ± 2.3 eV for $Re^+\text{-}O_2$.[1, 5, 48] Because there are no literature values available for the Re^+-S BDE for comparison, we use theoretical calculations of $D_0(Re^+\text{-}O_2)$ and $D_0(Re^+\text{-}S)$ to evaluate which species is actually formed (see below).

$ReSO^+$ thermochemistry

The threshold values for this channel in Tables 1 and 2 agree with each other within combined experimental uncertainties, but the MLOC model reproduces the experimental data better than the PST model and over a wider range, Figures 2 and 3. Using E_0 = 1.31 ± 0.12 eV (Table 2) in eq (2), we obtain $D_0(Re^+\text{-}SO)$ = 4.35 ± 0.14 eV, Table 3. Note that this value implies nothing about the structure of this product, which could be $ReSO^+$, $OReS^+$, or $ReOS^+$. Structural assignments can be evaluated by comparison with theory (see below).

Theoretical Results

In previous work, we have performed extensive calculations at several levels of theory on ReO^+ and ReO_2^+.[1, 4] The most pertinent results are listed in Table 3 for the comparison with the experimental data. Similar methods were employed here to evaluate the three lowest electronic states of ReS^+, and the B3LYP/def2-TZVPPD level was used to examine various states of $ReSO^+$ and $ReSO_2^+$

The ground state of ReS^+ was determined after including spin-orbit (S.O.) effects because theory produces values corresponding to the weighted average over J or Ω levels. We account for S.O. using a semi-empirical model given by $E^{SO} = A\ \Lambda\ M_S$,[1-4, 49-50] where A is the S.O. splitting constant, Λ is the molecular orbital angular momentum quantum number, and M_S is the molecular spin for a certain $\Omega = \Lambda + M_S$. Also, $E^{SO} = \sum a_i\ l_i \cdot s_i$ where a_i is the S.O. splitting constant for electron i (here, ζ_{5d}) and $l_i \cdot s_i$ is the dot product of the orbital angular momentum and spin of

electron *i*. This leads to S.O. corrections of 0.158, 0.00, and 0.316 eV for the $^5\Pi_{-1}$, $^3\Sigma^-$, and $^3\Delta_3$ states of ReS^+ (as detailed more fully for the analogous ReO^+ states previously).[1] When considering S.O. corrections to BDE values, the S.O. correction for the asymptotic products is also required. The lowest J levels for S, O, and Re^+ are 0.024, 0.010, and 0.000 eV, respectively, lower than the average of the weighted J levels.[51]

In the discussion below, the molecular orbital (mo) configurations discussed will only include valence electrons, such that core electrons of rhenium (1s–5s, 2p–5p, and 3d–4d) and of ligands (1s and 2s on O, and 1s, 2s, 2p, and 3s on S) are not specified. In general, for the diatomic species, 1σ and 1π are bonding mos, 1δ and 2σ (mostly 6s on the metal) are non-bonding mos, and 2π and 3σ are anti-bonding mos.

ReO^+

The BDE value for the ground state (GS) of ReO^+ ($^3\Delta_3$) calculated at the B3LYP/def2-TZVPPD level and including the S.O. correction is 4.70 eV. This value agrees reasonably well with the best experimental value of 4.82 ± 0.03 eV.[1] Other BDEs calculated at the B3LYP/aug-cc-pV5Z, BP86/aug-cc-pV5Z, and CCSD(T)/CBS levels are 4.82, 5.59, and 4.59 eV, respectively.[1] The previous study also found mean absolute deviations (MADs) relative to the experimental values of 0.23, 0.64, and 0.20 eV when using these three levels, respectively, when compared to BDEs for the MC^+ and MO^+ diatomic cations of M = Re, Os, and Ir.[4] Thus, the B3LYP and CCSD(T) levels are capable of providing reasonably accurate BDE values. Table 3 also lists the BDE calculated for the low-lying excited $^5\Pi_{-1}$ state, which is actually the GS before S.O. corrections are applied.[1] As seen here and in our previous work at multiple levels of theory, the experimental BDE agrees better with the theoretical values for the $^3\Delta_3$ ground state at B3LYP and CCSD(T) levels.

ReS^+

B3LYP/def2-TZVPPD theory indicates that the GS of ReS^+ is $^5\Pi$, Tables 3 – 4. After empirical

S.O. corrections, the GS is $^5\Pi_{-1}$ with a BDE of 3.67 eV. Excitation energies of a few low-lying states of ReS^+ were also calculated at various levels of theory and basis sets, Table 4 (see also Table S3 (ESI†) for more levels of theory and basis set combinations). These include $^3\Sigma^-$ and $^3\Delta$ states that lie 0.51 – 0.80 and 0.39 – 0.59 eV, respectively, higher than the $^5\Pi_{-1}$ GS (with S.O. corrections). The vibrational frequency of the $^3\Sigma^-$ state (555 – 612 cm^{-1}) is found to be higher than that of the GS (505 – 548 cm^{-1}), and the bond length (2.003 – 2.078 Å) is found to be shorter than the GS (2.069 – 2.087 Å). Likewise, the $^3\Delta$ state also has a higher frequency (593 – 618 cm^{-1}) and shorter bond length (2.007 – 2.018 Å) than the GS. Although all three states fully occupy the 1σ and 1π bonding mos, these differences occur because the high spin of the $^5\Pi$ GS requires occupation of an antibonding π∗ orbital ($1\delta^2 2\sigma^1 2\pi^{*1}$), whereas the $^3\Sigma^-$ or $^3\Delta$ states occupy only nonbonding orbitals ($1\delta^2 2\sigma^2$ or $1\delta^3 2\sigma^1$, respectively). Thus, the $^5\Pi$ GS has a lower bond order than the other two states. Theoretical BDE values for the $^5\Pi_{-1}$ GS of ReS^+ (Table S3, ESI†) predict a threshold for formation of $ReS^+ + O_2$ between 1.2 – 2.6 eV, well above the apparent threshold near 0.2 eV. This clearly suggests that ReS^+ is not formed experimentally at the threshold observed here. Because this species does not appear to be involved, further investigation of higher lying states of ReS^+ was not performed in the current study.

ReO_2^+

As shown in Table 3, at the B3LYP/def2-TZVPPD level, the ground state of ReO_2^+ is found to be $^3B_1$ with a BDE for loss of molecular oxygen (Re^+-O_2) of 5.00 eV,[1] compared with the experimental value of 5.75 ± 0.02 eV. Although this deviation of 0.75 eV is relatively large, it is much smaller than the 2.08 eV deviation obtained for ReS^+, such that it is reasonable to assign ReO_2^+ as the experimentally formed species. Further, if the thermochemistry of this species is designated by the ORe^+-O BDE, better agreement is obtained as theory predicts a value of 5.53 eV (at the B3LYP/def2-TZVPPD level; 5.83 eV without S.O. correction) and the present experimental result is 6.05 ± 0.05 eV. The discrepancy here (0.52 eV) is smaller because the $D_0(Re^+$-$O_2)$ comparison (0.75 eV difference) includes differences between theory and experiment for $D_0(Re^+$-

O) (see above) and $D_0(O_2)$.

$ReSO^+$

The lowest energy structure of the $ReSO^+$ product calculated at the B3LYP/def2-TZVPPD level is found to be an $OReS^+$ inserted structure having a $^3A''$ GS with a Re^+-SO BDE of 3.74 eV and a ORe^+-S BDE of 4.44 eV. This species has a S.O. correction of zero. These theoretical values are in modest agreement with the experimental values of 4.35 ± 0.14 and 4.89 ± 0.19 eV, respectively, Table 3. The discrepancies are not unlike those for D_0(OS-O) and D_0(S-O_2) of 0.40 and 0.49 eV, Table S2 (ESI†).

Various geometries and states calculated for $ReSO^+$ are shown in Table 5. Among the inserted structures of $ReSO^+$ (∠SReO > 100°), $^3A''$ is found to be the most stable state followed by $^1A'$ (0.19 eV higher), $^5A''$ (at 1.30 eV), and $^7A''$ (at 3.27 eV). The high-spin septet state allows little covalent bonding between Re^+ and the O and S ligands, accounting for its high energy. In general, among the inserted structures, lower multiplicity is associated with higher vibrational frequencies, consistent with increasing covalent interactions. The highest frequencies (Re-O stretch) for the $^3A''$ and $^5A''$ states (1027 and 1038 cm^{-1}, respectively) are similar to the isolated ReO^+ ($^5\Pi$) state (1015 cm^{-1}),[1] whereas that for the singlet state is higher (1077 cm^{-1}). The medium frequencies (Re-S stretch, 560, 398, and 582 cm^{-1}, respectively) are quite different from the isolated ReS^+ ($^5\Pi$) (505 cm^{-1}). The Re-O bond lengths of the $^3A''$ and $^5A''$ states (1.667 and 1.663 Å, respectively) are also similar to the isolated ReO^+ ($^5\Pi$) (1.679 Å),[1] whereas that for the singlet state is shorter (1.648 Å).

In side-on structures of $ReSO^+$ (36° < ∠SReO < 50°), the oxygen atom is closer to the rhenium than the sulfur atom by 0.20 – 0.76 Å, which is similar to the difference in their covalent radii, 0.66 Å for O and 1.05 Å for S.[52] Of these structures, $^5A'$ (2.00 eV higher than the $^3A''$ $OReS^+$ GS) is found to be the most stable followed by $^3A''$ (at 2.53 eV), $^7A''$ (at 2.67 eV), and then $^1A'$ (at 3.30 eV). Finally, end-on structures of $ReSO^+$ (∠SReO = 0°), were also located, Table 5. For both $^3\Sigma^-$ and $^1\Gamma$ states, the $ReSO^+$ structure (S attached to the metal) is more stable than $ReOS^+$ (O attached to the metal) by 0.21 and 0.82 eV, respectively. The $^3\Sigma^-$ state is more stable than the $^1\Gamma$

state for both geometries. The most unperturbed S-O bond can be found in the $ReOS^+$ ($^1\Gamma$) end-on structure as it has a vibrational frequency (1137 cm^{-1}) that is very similar to that calculated for isolated SO (1145 cm^{-1}), Table 1.

Potential energy surfaces of $ReSO_2^+$

The PESs of the $ReSO_2^+$ system were investigated at the B3LYP/def2-TZVPPD level for septet, quintet, and triplet spin surfaces. These are shown in Figure 4 with the corresponding structure of each intermediate and transition state displayed in Figure 5. The geometrical parameters of these structures along with those of reactants and products are listed in Table S4 (ESI†). In the following, intermediates **1** refer to Re^+OSO or Re^+O_2S adducts, **2** refers to ORe^+SO intermediates, **3** to ORe^+OS intermediates, and **4** to SRe^+O_2 intermediates.

Septet surfaces. Ground state (GS) reactants, Re^+ (^7S) + SO_2 ($^1A_1$), can couple to form two versions of the Re^+OSO adduct, both of which are planar. In ^{7}**1'** ($^7A'$), one oxygen of SO_2 attaches to the metal with the second oxygen being much farther away, r(Re-O) = 4.285 Å. ^{7}**1'** is 0.72 eV lower than GS reactants. The SO_2 is nearly unperturbed by the metal as the vibrational frequencies of SO_2 (Table S4, ESI†) are similar to isolated SO_2, Table S2 (ESI†). GS reactants can also couple to form ^{7}**1** ($^7A''$), having shorter ReO bond distances. This structure lies 0.39 eV below GS reactants. Here, the tighter binding perturbs the SO_2 ligand, with vibrational frequencies that are significantly different from those in molecular SO_2, Tables S2 and S4 (ESI†). ^{7}**1'** and ^{7}**1**, which have different C_S symmetries, can interconvert through a nonplanar transition state (^{7}**TS1'/1**) that lies 0.37 eV lower than the GS reactants (only 0.02 eV above ^{7}**1**). The imaginary frequency of this TS (-83 cm^{-1}) corresponds primarily to changing the length of the longer Re-O bond.

From either of the septet $Re^+(SO_2)$ adducts, the Re^+O-SO bond can be cleaved to form ReO^+ ($^5\Pi$) + SO ($^3\Sigma^-$) products, calculated to lie 0.69 eV above GS reactants. Note that this is an excited state product, as the GS ReO^+ ($^3\Delta$) + SO ($^3\Sigma^-$) products cannot be formed from septet intermediates while conserving spin. As this cleavage occurs, it is also possible for the incipient SO product to migrate to the Re^+ cation via ^{7}**TS1/2** forming the ORe^+SO intermediate, ^{7}**2**, lying

1.15 and 0.11 eV above GS reactants, respectively. The imaginary vibration (-211 cm^{-1}) in ^{7}**TS1/2** shows a concerted S-O and Re-O bond-breaking and Re-S bond-forming process. From intermediate ^{7}**2**, loss of the SO ligand can again lead to formation of the ReO^+ ($^5\Pi$) + SO ($^3\Sigma^-$) products, or cleavage of the S-O bond yields $OReS^+$ (^{5}A") + O (^{3}P), 2.81 eV above GS reactants and 1.30 eV above $OReS^+$ (^{3}A″) + O (^{3}P) GS products.

From ^{7}**1**, activation of an S-O bond leads to transition state ^{7}**TS1/3** (^{7}A″), which lies 0.38 eV above GS reactants. In this TS, the imaginary vibration (-190 cm^{-1}) shows a concerted S-O bond-breaking, Re-O bond-making process leading to the intermediate, ^{7}**3**, ORe^+OS. This intermediate lies 0.71 eV below GS reactants. ^{7}**3** can rearrange by transferring the sulfur to the rhenium cation via ^{7}**TS3/4** (1.35 eV above GS reactants). This forms the $SReO_2^+$ intermediate ^{7}**4**, which lies 1.31 eV above GS reactants and, like ^{7}**TS3/4**, is nonplanar. The imaginary frequency in ^{7}**TS3/4** (-138 cm^{-1}) corresponds to concerted S-O bond-breaking and Re-S bond-forming motions. In spin conserving reactions, the ^{7}**3** intermediate can dissociate either to ReO^+ ($^5\Pi$) + SO ($^3\Sigma^-$) or $ReOS^+$ (^{5}A') + O (^{3}P), and ^{7}**4** can form $OReS^+$ (^{5}A") + O (^{3}P), but all these products are excited species calculated to lie 0.69, 3.51, and 2.81 eV above GS reactants. These energies are well above the thresholds observed in the experiment, Table 1 and 2. This result indicates that the surfaces evolving from GS reactants must couple with surfaces of different spin in order to form products at the experimental thresholds. Thus, spin is not a good quantum number because of the extensive S.O. coupling, a result also found in other Re^+ reaction systems.[4, 14-15]

Quintet surfaces. The quintet spin surface shown in Figure 4 starts from Re^+ (^{5}D) + SO_2 ($^1A_1$) reactants (2.12 eV higher than GS reactants, compared to 1.827 eV from experiment[51]). These couple to form the nonplanar ^{5}**1'** Re^+OSO adduct with one O bound to the metal. This state lies 0.74 eV lower than GS reactants and 0.02 eV below ^{7}**1'**. ^{5}**1'** exhibits significant differences in SO_2 vibrational modes compared to molecular SO_2, Tables S2 and S4 (ESI†). Because the ^{5}**1'** and ^{7}**1'** intermediates are close in energy, these adducts are a plausible place for the system to change to the lower spin state needed to form products in their GSs. From ^{5}**1'**, an S-O bond can be activated by passing over ^{5}**TS1'/3,** which lies 0.32 eV above GS reactants (only 0.06 eV below the septet

spin analogue, ^{7}**TS1/3**). ^{5}**TS1'/3** is substantially more compact than ^{7}**TS1/3**, a consequence of the stronger bonds allowed by the lower spin state. The imaginary frequency (-519 cm^{-1}) again shows cleavage of an S-O bond synchronously with formation of a Re-O bond. This process forms ^{5}**3** $ORe^{+}OS$, which lies 1.94 eV below GS reactants. This intermediate can dissociate readily in spin-allowed processes to form the GS product asymptotes, ReO^{+} ($^{3}\Delta$) + SO ($^{3}\Sigma^{-}$) (by cleaving the Re-O bond) and ReO_2^{+} ($^{3}B_1$) + S (^{3}P) (by cleaving the S-O bond). These products are calculated to lie 0.57 and 0.39 eV above the ground state reactants, respectively (compared to experimental values of 0.88 ± 0.05 and 0.15 ± 0.02 eV, respectively). The ^{5}**3** intermediate can also dissociate to an excited state product asymptote, ReO^{+} ($^{5}\Pi$) + SO ($^{3}\Sigma^{-}$), 0.69 eV above the GS products.

Alternatively, ^{5}**3** can rearrange by passing over ^{5}**TS3/4** that lies 0.77 eV below GS reactants. In this TS, the S-O bond breaks allowing generation of a Re-S bond. The imaginary vibration (-415 cm^{-1}) shows this concerted motion and forms intermediate ^{5}**4** $SRe^{+}O_2$ ($^{5}B_2$), in which all three ligands are bound directly to the metal. This intermediate lies 1.59 eV lower than GS reactants and is a planar structure with C_{2v} symmetry. The Re-S bond length is particularly long, 2.611 Å, compared to 2.087 Å in isolated ReS^{+} ($^{5}\Pi$), whereas the Re-O bonds are similar to those of ReO_2^{+} ($^{3}B_1$), 1.669 Å. ^{5}**4** can dissociate readily by cleaving the Re-S bond to form ReO_2^{+} ($^{3}B_1$) + S (^{3}P) or by cleaving a Re-O bond to form $OReS^{+}$ ($^{3}A''$) + O (^{3}P). Both processes are spin-allowed along the quintet surface and are calculated to lie 0.39 and 1.51 eV, respectively, above GS reactants. These values agree well with the experimental onsets for both processes, 0.15 ± 0.02 and 1.31 ± 0.12 eV, respectively.

Triplet surface. The triplet spin surface shown in Figure 4 starts from Re^{+} (^{3}H) + SO_2 ($^{1}A_1$) reactants (2.97 eV above GS reactants, compared to 3.21 eV found experimentally[51]). Different from the septet and quintet surfaces, all of the triplet intermediates and transition states are nonplanar. The triplet reactants couple to form the ^{3}**1'** $Re^{+}OSO$ adduct with one O bound to the metal. ^{3}**1'** lies 0.34 eV above GS reactants, and similar to ^{5}**1'**, exhibits significant differences in SO_2 vibrational modes compared to molecular SO_2, Tables S2 and S4 (ESI†). From ^{3}**1'**, the adduct can form a second Re-O bond by passing over ^{3}**TS1'/1**, only 0.01 eV above ^{3}**1'**, yielding ^{3}**1**, 0.07 eV below

GS reactants. In ^{3}**1**, both oxygens are attached symmetrically to both Re and S such that the adduct has C_S symmetry. Intermediate ^{3}**1** can rearrange to ^{3}**3** ORe^+OS (2.30 eV below GS reactants) via ^{3}**TS1/3** (0.14 eV above GS reactants) in which one of the SO bonds is broken (imaginary frequency of -361 cm^{-1}). From intermediate ^{3}**3**, passing over ^{3}**TS3/4** forms SRe^+O_2 ^{3}**4,** the global minimum intermediate among all three spin states considered here, 3.30 eV below GS reactants. ^{3}**TS3/4** lies 1.56 eV below GS reactants, and the imaginary frequency (-672 cm^{-1}) shows synchronous S-O bond-cleavage and Re-S bond-formation. Compared to ^{5}**4**, the Re-S bond length for ^{3}**4** is much shorter (2.611 Å versus 2.237 Å), and more similar to the isolated ReS^+ bond length (2.087 Å for $^5\Pi$). The ^{3}**4** intermediate can dissociate to GS products by cleaving the Re-S bond to form ReO_2^+ ($^3B_1$) + S (^{3}P) or by cleaving a Re-O bond to form $OReS^+$ ($^3A''$) + O (^{3}P) (0.39 and 1.51 eV above GS reactants, respectively). This intermediate could also yield ReS^+ ($^5\Pi$) + O_2 ($^3\Sigma^-$) by bringing the two oxygen atoms together. There is no additional TS or barrier observed during this process. We also examined the formation of ReS^+ ($^5\Pi$) + 2O (^{3}P) formed by cleaving the Re-O bond in the $OReS^+$ ($^3A''$) product. Although not shown in Figure 4 because the energy is 6.97 eV above GS reactants, this process also exhibits no additional TS or barrier in excess of the product asymptote.

Discussion

Comparison of metal oxide and metal sulfide BDEs

The experimental BDEs of Re^+-O and ORe^+-O are 4.82 ± 0.03[1] and 6.05 ± 0.05 eV, respectively, and that for ORe^+-S is 4.89 ± 0.19 eV. Although we also measure $D_0(Re^+\text{-SO})$ = 4.35 ± 0.14 eV, because $D_0(Re^+\text{-S})$ is not available experimentally, an experimental value for $D_0(SRe^+\text{-O})$ cannot be formulated. With theoretical calculations at the B3LYP/def2-TZVPPD level, the BDEs of three rhenium-oxide cation species were determined as 4.70 (Re^+-O), 5.53 (ORe^+-O), and 5.44 (SRe^+-O) eV (4.42, 5.83, and 5.62 eV without S.O. correction, respectively), with the former two in reasonable agreement with experiment. A similar theoretical comparison can be made for the comparable rhenium-sulfide BDEs of ReS^+ and $OReS^+$. The BDEs of Re^+-S and ORe^+-S are calculated as 3.67 and 4.44 eV, respectively (3.52 and 4.72 eV without S.O. correction,

respectively), with the latter in reasonable agreement with experiment. Not unexpectedly, the two sulfide BDEs are weaker than the oxide counterparts by ~1.0 eV. Perhaps surprisingly, these comparisons indicate that the triatomic species have stronger bonds than the diatomic cations. This can be understood on the basis of promotion energies needed to put the metal cation into an appropriate electronic configuration for bonding. For both ReO^+ and ReS^+, both the $^5\Pi$ and $^3\Delta$ states diabatically correlate with Re^+ in its ^5G [$5d^5(^4G)6s$] state (where two of the 5d electrons are low-spin coupled). This state (average over all S.O. levels) lies 2.56 eV above the ^7S [$5d^5(^6S)6s$] ground state.[51] If this promotion energy is added to the ReO^+ and ReS^+ BDEs, then the first ligand BDEs are 1.4 – 1.8 eV greater than the second ligand BDEs. This is consistent with the calculated bond lengths, 1.61 Å for Re^+-O ($^3\Delta$) versus 1.67 Å for ORe^+-O ($^3B_1$) and 2.01 Å for Re^+-S ($^3\Delta$) versus 2.08 Å for ORe^+-S ($^3A''$). The $^5\Pi$ states of ReO^+ and ReS^+ have longer bonds, 1.68 and 2.09 Å, respectively, which occurs because this state has an electron occupying a π^* antibonding orbital, thus lowering the bond order to 2.5 from that in the $^3\Delta$ state of 3.0.

Access of surfaces towards products

Like the $Re^+ + CO$ reaction, spin-allowed processes in the $Re^+ + SO_2$ reaction are limited by the singlet spin of the reactant neutral. As shown in Figure 4, formation of all ground state products from ground state reactants requires at least one spin-forbidden transition. The correlation of these pathways is shown in eqs (7) – (12) (cut arrows indicate spin-forbidden transitions).

$$Re^+ (^7S) + SO_2 (^1A_1) \rightarrow ReSO_2^+ (^7A) \text{–X→ } ReO^+ (^3\Delta) + SO (^3\Sigma^-) \quad (7)$$

$$\text{–X→ } ReO_2^+ (^3B_1) + S (^3P) \quad (8)$$

$$\text{–X→ } OReS^+ (^3A'') + O (^3P) \quad (9)$$

$$\text{–X→ } ReSO_2^+ (^{5,3,1}A) \rightarrow ReO^+ (^3\Delta) + SO (^3\Sigma^-) \quad (10)$$

$$\rightarrow ReO_2^+ (^3B_1) + S (^3P) \quad (11)$$

$$\rightarrow SReS^+ (^3A'') + O (^3P) \quad (12)$$

Because ground state products appear to be formed experimentally for all three products, all reactions must proceed by adiabatic pathways that do not conserve spin.

The PESs in Figure 4 indicate that the GS reactants evolve along the septet surfaces to form either the ^{7}**1′** or ^{7}**1** $Re^{+}(SO_2)$ adducts. Spin conversion to the quintet surface is possible for ^{7}**1′** because of the proximity of ^{5}**1′**, and likewise conversion to the triplet surface is feasible for ^{7}**1** because ^{3}**1** is nearby. If the system remained on the septet surface, it might also form ^{7}**3**, which could plausibly convert to either the quintet or triplet analogues that lie at lower energies. According to the overall calculated PESs, it appears that the ^{7}**TS1/3**, ^{5}**TS1′/3**, or ^{3}**TS1/3** transition states are rate limiting, because once the $ORe^{+}OS$ (**3**) intermediates are formed, conversion between **3** and **4** ($SRe^{+}O_2$) on the quintet and triplet surfaces should be facile and these intermediates lead to the ground states of all three observed products with no barriers in excess of the product asymptotes. The lowest of these TSs is ^{3}**TS1/3** at 0.14 eV above GS reactants, whereas ^{5}**TS1′/3** and ^{7}**TS1/3** lie at 0.32 and 0.38 eV. According to theory, none of these TSs would perturb the threshold for formation of the lowest energy product, ReO_2^{+} ($^{3}B_1$) + S (^{3}P) at 0.39 eV. It also seems feasible that excited states of the various products could be formed, but there are no specific indications in the observed cross sections that suggest such higher energy onsets

Comparison of ReO^{+} formation cross sections with previous studies

As noted in the introduction, previous GIB studies of O_2 with M^{+} (M^{+} = Re^{+}, Os^{+}, and Ir^{+}) exhibited two endothermic features in the cross sections of the MO^{+} products,[1-3] whereas reactions of these metal cations with CO yielded only a single feature,[4] as is also found in the present reaction with SO_2. This is apparent in Figure 6, which overlays the ReO^{+} cross sections from studies of all three gases (SO_2, O_2, and CO) by aligning the data at the neutral BDEs such that the x-axis becomes "energy (CM) – D_0," where D_0 is the BDE of OS-O, O-O, or C-O. On this energy scale, it can be seen that all three reactions are endothermic and exhibit the same apparent threshold, consistent with formation of ground state ReO^{+} in all three systems. Further, all three cross sections begin to decline more rapidly at 0 eV on this scale, i.e., at D_0 on the CM scale.

One motivation for the studies with CO and SO_2 was to better understand the unusual dual features observed in the O_2 reaction. Our original work ruled out the possibilities that these features

could be attributed to reactions of different electronic states of Re^+ or formation of different states of the O product neutral. In other studies, we have observed multiple features in cross sections when formation of the ground state of the product ion is spin-forbidden, but formation of an excited state is spin-allowed,[53-55] or ground state products are formed via intermediates that require a spin-forbidden process at low energies and a spin-allowed process at higher energies.[56] However, the Re^+ (^7S) + O_2 ($^3\Sigma_g^-$) → ReO^+ ($^3\Delta$) + O (^3P) reaction is spin-allowed, whereas in the CO and SO_2 systems, formation of GS ReO^+ ($^3\Delta$) is spin-forbidden because of the singlet spin of the neutral reactants. Thus, spin conservation cannot explain the two features in the O_2 reaction.

One final suggestion for the two features in the O_2 reactions of Re^+, Os^+, and Ir^+ focused on the fact that for this triatomic system, C_S symmetry can be maintained throughout the reaction. Quantum chemical calculations showed that the behavior of the A′ and A″ surfaces was qualitatively different in all three systems, with one of them (A′ for Re^+, and A″ for Os^+ and Ir^+) exhibiting no low-energy pathways to the formation of the metal dioxide cation intermediates needed to form the final MO^+ + O products. Thus, for Re^+ + O_2, the low-energy behavior could correspond to adiabatic reactions along the favorable A″ surfaces, with the high energy feature associated with reaction along the A′ surface or coupling between the A′ and A″ surfaces at high energies. Such coupling can occur at elevated kinetic energies by Coriolis (electronic-rotational) coupling, as we have observed for reactions of state-specific reactions of Ar^+, Kr^+, and Xe^+ with H_2 and its isotopomers (HD and D_2) above 1−2 eV collision energies.[18, 57-58] The reactions of M^+ with CO were expected to test this hypothesis because these triatomic systems also have C_S symmetry; however, only one feature in the MO^+ cross sections was observed, Figure 6. Here, because the CO bond energy is nearly twice that of O_2, the system reaches the high energies that permit Coriolis coupling before the endothermicity of the reaction to form MO^+. Hence, only one feature is observed. In the SO_2 reaction studied here, the endothermicity of the oxidation reaction is similar to that in the O_2 system, but this four-atom reaction is no longer restricted to a plane, such that all surfaces have A (C_1) symmetry in all collisions (even if particular intermediates have higher symmetry at their minima). Thus, the observation of a single feature in the present study is

consistent with the hypothesis of adiabatic/diabatic behavior evolving from the plane of symmetry in the triatomic reactions of $M^+ + O_2$.

More detailed comparison of the ReO^+ cross sections in Figure 6 suggests that the behavior of the SO_2 cross section at low energy is more similar to the first feature in the O_2 cross section in that both rise rapidly from the common threshold associated with ground state product formation. The differences in this behavior can probably be attributed to the very low endothermicity of the O_2 reaction, 0.29 ± 0.03 eV, compared to the higher 0.88 ± 0.05 eV threshold measured here (Table 2). The assumed model for this low energy feature in the O_2 system also exhibited a slow decline in the cross section as the collision energy increased further (until it reached $D_0(O_2)$, where it declined more rapidly, consistent with the behavior observed here. Likewise, the behavior of the high energy feature in the O_2 cross section is similar to that of the CO cross section, which is consistent with the high energy required for the latter reaction.

Conclusion

The $Re^+ + SO_2$ reaction has been investigated using guided ion beam tandem mass spectrometry. This study is an extension of previous work on MO^+ formation in $M^+ + O_2$ and $M^+ + CO$ reactions (M = Re, Os, and Ir).[1-4] Formation of MO^+ in the O_2 reactions exhibited two distinct endothermic features for all three metal cations, whereas the cross sections for MO^+ formed in CO and SO_2 (M = Re only) reactions exhibited only one feature. These systems can be compared and contrasted as follows. 1) The BDEs of O_2 and SO_2 are comparable to each other whereas that of CO is significantly higher, such that the formation of ReO^+ occurs at much higher collision energies in the latter system. 2) CO and SO_2 have singlet spin states, in contrast to the triplet state for O_2, such that formation of ReO^+ is spin forbidden in the first two systems, but spin-allowed in the reaction with O_2. Despite these restrictions, the threshold for ReO^+ formation in all three reactions corresponds to formation of ground state ReO^+. Thus, the CO and SO_2 results demonstrate that spin is not a good quantum number for a heavy metal system like Re, and that spin constraints cannot rationalize the origin of the two features observed in the O_2 reaction. 3) A

plane of symmetry exists in the triatomic O_2 and CO reactions, but does not in the four-atom SO_2 reactions. Quantum chemical calculations indicate that the reaction of $Re^+ + O_2$ can only occur at low energies on surfaces of A″ symmetry, such that the higher energy feature may correspond to reactions on the A′ surfaces or coupling of rotational and electronic modes (Coriolis). As the four-atom $Re^+ + SO_2$ system is not confined to a plane, such restrictions are not operative in this system. For CO, because the formation of ReO^+ can only occur at high energies, coupling between A′ and A″ surfaces may already occur at the thermodynamic threshold. Further tests of this concept can involve the examination of the reactions of Os^+ and Ir^+ with SO_2 for comparison with the present results and their reactions with O_2 and CO.

Other products, ReO_2^+ and $ReSO^+$, were also observed in the $Re^+ + SO_2$ reaction and were evaluated to determine BDEs for Re^+-O_2, ORe^+-O, Re^+-SO, and ORe^+-S. BDEs for diatomic (Re^+-O and Re^+-S) and triatomic (ORe^+-O, SRe^+-O, and ORe^+-S) products were compared using both experimental (when available) and theoretical approaches. Oxide BDEs are stronger than the sulfide BDEs for analogous molecules and BDEs in the triatomic species are found to be greater than those in the diatomic products, which can be explained by the promotion energy of atomic Re^+ required to allow the metal cation to bind strongly to O and S.

Conflicts of interest

The authors declare no competing financial interest.

Acknowledgements

This research is funded by the National Science Foundation under Grant No. CHE-1664618. The theoretical calculations are expedited by facilities provided by the Center for High Performance Computing (CHPC) at the University of Utah. Professor Michael D. Morse is thanked for many helpful discussions concerning S.O. coupling.

References

1. Armentrout, P. B. The Bond Energy of ReO^+: Guided Ion-Beam and Theoretical Studies of the Reaction of Re^+ (^7S) with O_2. *J. Chem. Phys.* **2013,** *139*, 084305.
2. Hinton, C. S.; Citir, M.; Armentrout, P. B. Guided Ion-Beam and Theoretical Studies of the Reaction of Os^+ (^6D) with O_2: Adiabatic and Nonadiabatic Behavior. *Int. J. Mass Spectrom.* **2013,** *354-355*, 87-98.
3. Armentrout, P. B.; Li, F.-X. The Bond Energy of IrO^+: Guided Ion-Beam and Theoretical Studies of the Reaction of Ir^+ (^5F) with O_2. *J. Phys. Chem. A* **2013,** *117*, 7754-7766.
4. Kim, J.; Cox, R. M.; Armentrout, P. B. Guided Ion Beam and Theoretical Studies of the Reactions of Re^+, Os^+, and Ir^+ with CO. *J. Chem. Phys.* **2016,** *145*, 194305.
5. Johnson III, R. D. NIST Computational Chemistry Comparison and Benchmark Database. NIST Computational Chemistry Comparison and Benchmark Database (2018); http://cccbdb.nist.gov/ (accessed April 12, 2018).
6. Loh, S. K.; Hales, D. A.; Lian, L.; Armentrout, P. B. Collision-Induced Dissociation of Fe_n^+ (n = 2 - 10) with Xe: Ionic and Neutral Iron Cluster Binding Energies. *J. Chem. Phys.* **1989,** *90*, 5466-5485.
7. Schultz, R. H.; Armentrout, P. B. Reactions of N_4^+ with Rare Gases from Thermal to 10 eV c.m.: Collision-Induced Dissociation, Charge Transfer, and Ligand Exchange. *Int. J. Mass Spectrom. Ion Processes* **1991,** *107*, 29-48.
8. Clemmer, D. E.; Chen, Y.-M.; Khan, F. A.; Armentrout, P. B. State-Specific Reactions of Fe^+(a^6D, a^4F) with D_2O and Reactions of FeO^+ with D_2. *J. Phys. Chem.* **1994,** *98*, 6522-6529.
9. Haynes, C. L.; Armentrout, P. B. Thermochemistry and Structures of $CoC_3H_6^+$: Metallacycle and Metal-Alkene Isomers. *Organomet.* **1994,** *13*, 3480-3490.
10. Kickel, B. L.; Armentrout, P. B. Guided Ion Beam Studies of the Reactions of Group 3 Metal Ions (Sc^+, Y^+, La^+, and Lu^+) with Silane. Electronic State Effects, Comparison to Reactions with Methane, and M^+-SiH_x (x = 0 - 3) Bond Energies. *J. Am. Chem. Soc.* **1995,** *117*, 4057-4070.
11. Kickel, B. L.; Armentrout, P. B. Reactions of Fe^+, Co^+ and Ni^+ with Silane. Electronic State Effects and M^+-SiH_x (x = 0 - 3) Bond Energies. *J. Am. Chem. Soc.* **1995,** *117*, 764-773.
12. Chen, Y.-M.; Elkind, J. L.; Armentrout, P. B. Reactions of Ru^+, Rh^+, Pd^+, and Ag^+ with H_2, HD and D_2. *J. Phys. Chem.* **1995,** *99*, 10438-10445.
13. Sievers, M. R.; Chen, Y.-M.; Elkind, J. L.; Armentrout, P. B. Reactions of Y^+, Zr^+, Nb^+, and Mo^+ with H_2, HD, and D_2. *J. Phys. Chem.* **1996,** *100*, 54-62.
14. Armentrout, P. B.; Li, F.-X. Probes of Spin-conservation in Heavy Metal Reactions: Experimental and Theoretical Studies of the Reactions of Re^+ with H_2, D_2, and HD. *J. Chem. Phys.* **2004,** *121*, 248-256.
15. Armentrout, M. M.; Li, F.-X.; Armentrout, P. B. Is Spin Conserved in Heavy Metal Systems? Experimental and Theoretical Studies of the Reaction of Re^+ with Methane. *J. Phys. Chem. A* **2004,** *108*, 9660-9672.
16. Teloy, E.; Gerlich, D. Integral Cross Sections for Ion-Molecule Reactions. 1. The Guided Beam Technique. *Chem. Phys.* **1974,** *4*, 417-427.
17. Gerlich, D. Inhomogeneous rf Fields: A Versatile Tool for the Study of Processes with Slow Ions. *Adv. Chem. Phys.* **1992,** *82*, 1-176.
18. Ervin, K. M.; Armentrout, P. B. Translational Energy Dependence of $Ar^+ + XY \rightarrow ArX^+ + Y$ (XY = H_2, D_2, HD) from Thermal to 30 eV c.m. *J. Chem. Phys.* **1985,** *83*, 166-189.

19. Daly, N. R. Scintillation Type Mass Spectrometer Ion Detector. *Rev. Sci. Instrum.* **1960,** *31*, 264-267.
20. Chantry, P. J. Doppler Broadening in Beam Experiments. *J. Chem. Phys.* **1971,** *55*, 2746-2759.
21. Lifshitz, C.; Wu, R. L. C.; Tiernan, T. O.; Terwilliger, D. T. Negative Ion-molecule Reactions of Ozone and Their Implications on the Thermochemistry of O_3^-. *J. Chem. Phys.* **1978,** *68*, 247-260.
22. Weber, M. E.; Elkind, J. L.; Armentrout, P. B. Kinetic Energy Dependence of $Al^+ + O_2 \rightarrow AlO^+ + O$. *J. Chem. Phys.* **1986,** *84*, 1521-1529.
23. Chesnavich, W. J.; Bowers, M. T. Statistical phase space theory of polyatomic systems: Rigorous energy and angular momentum conservation in reactions involving symmetric polyatomic species. *J. Chem. Phys.* **1977,** *66*, 2306-2315.
24. Webb, D. A.; Chesnavich, W. J. Multiple transition state models for the reactions atomic C^+ (D_2,D) CD^+ and C^+ (H_2,H) CH^+. *J. Phys. Chem.* **1983,** *87*, 3791-3798.
25. Ervin, K. M.; Armentrout, P. B. $C^+(^2P) + H_2(D_2,HD) \rightarrow CH^+(CD^+) + H(D)$ II. Statistical phase space theory. *J. Chem. Phys.* **1986,** *84*, 6750-6760.
26. Gioumousis, G.; Stevenson, D. P. Reactions of Gaseous Molecule Ions with Gaseous Molecules. V. Theory. *J. Chem. Phys.* **1958,** *29*, 294-299.
27. Talrose, V. L.; Vinogradov, P. S.; Larin, I. K., On the Rapidity of Ion-molecule Reactions. In *Gas Phase Ion Chemistry*, Bowers, M. T., Ed. Academic: New York, 1979; Vol. 1, pp 305-347.
28. Armentrout, P. B.; Simons, J. Understanding Heterolytic Bond Cleavage. *J. Am. Chem. Soc.* **1992,** *114*, 8627-8633.
29. Frisch, M. J.; Trucks, G. W.; Schlegel, H. B.; Scuseria, G. E.; Robb, M. A.; Cheeseman, J. R.; Scalmani, G.; Barone, V.; Mennucci, B.; Petersson, G. A., et al. *Gaussian 09, Revision D.01* Gaussian, Inc.: Wallingford, CT, USA, 2009.
30. Lee, C.; Yang, W.; Parr, R. G. Development of the Colle-Salvetti Correlation-Energy Formula into a Functional of the Electron Density. *Phys. Rev. B* **1988,** *37*, 785-789.
31. Becke, A. D. Density-functional Thermochemistry. III. The Role of Exact Exchange. *J. Chem. Phys.* **1993,** *98*, 5648-5652.
32. Raghavachari, K.; Trucks, G. W.; Pople, J. A.; Head-Gordon, M. A Fifth-order Perturbation Comparison of Electron Correlation Theories. *Chem. Phys. Lett.* **1989,** *157*, 479-483.
33. Bartlett, R. J.; Watts, J. D.; Kucharski, S. A.; Noga, J. Non-iterative Fifth-order Triple and Quadruple Excitation Energy Corrections in Correlated Methods. *Chem. Phys. Lett.* **1990,** *165*, 513-522.
34. Scuseria, G. E.; Lee, T. J. Comparison of Coupled-cluster Methods Which Include the Effects of Connected Triple Excitations. *J. Chem. Phys.* **1990,** *93*, 5851-5855.
35. Crawford, T. D.; Stanton, J. F. Investigation of an Asymmetric Triple-Excitation Correction for Coupled-Cluster Energies. *Int. J. Quantum Chem.* **1998,** *70*, 601-611.
36. Li, F.-X.; Zhang, X.-G.; Armentrout, P. B. The Most Reactive Third-row Transition Metal: Guided Ion Beam and Theoretical Studies of the Activation of Methane by Ir^+. *Int. J. Mass Spectrom.* **2006,** *255/256*, 279-300.
37. Armentrout, P. B.; Parke, L.; Hinton, C.; Citir, M. Activation of Methane by Os^+: Guided Ion Beam and Theoretical Studies. *ChemPlusChem* **2013,** *78*, 1157-1173.

38. Andrae, D.; Haeussermann, U.; Dolg, M.; Stoll, H.; Preuss, H. Energy-adjusted Ab Initio Pseudopotentials for the Second and Third Row Transition Elements. *Theor. Chim. Acta* **1990,** *77*, 123-141.
39. Weigend, F.; Ahlrichs, R. Balanced Basis Sets of Split Valence, Triple Zeta Valence and Quadruple Zeta Valence Quality for H to Rn: Design and Assessment of Accuracy. *Phys. Chem. Chem. Phys.* **2005,** *7*, 3297-3305.
40. Figgen, D.; Peterson, K. A.; Dolg, M.; Stoll, H. Energy-consistent Pseudopotentials and Correlation Consistent Basis Sets for the 5d Elements Hf-Pt. *J. Chem. Phys.* **2009,** *130*, 164108.
41. Feller, D. The Role of Databases in Support of Computational Chemistry Calculations. *J. Comput. Chem.* **1996,** *17*, 1571-1586.
42. Schuchardt, K. L.; Didier, B. T.; Elsethagen, T.; Sun, L.; Gurumoorthi, V.; Chase, J.; Li, J.; Windus, T. L. Basis Set Exchange: A Community Database for Computational Sciences. *J. Chem. Inf. Model.* **2007,** *47*, 1045-1052.
43. Halkier, A.; Helgaker, T.; Jørgensen, P.; Klopper, W.; Koch, H.; Olsen, J.; Wilson, A. K. Basis-set convergence in correlated calculations on Ne, N_2, and H_2O. *Chem. Phys. Lett.* **1998,** *286*, 243-252.
44. Halkier, A.; Helgaker, T.; Jørgensen, P.; Klopper, W.; Olsen, J. Basis-set convergence of the energy in molecular Hartree–Fock calculations *Chem. Phys. Lett.* **1999,** *302*, 437-446.
45. Gdanitz, R. J.; Cardoen, W.; Windus, T. L.; Simons, J. Very Large Scale Computations of the Free Energies of Eight Low-Lying Structures of Arginine in the Gas Phase. *J. Phys. Chem. A* **2004,** *108*, 515 – 518.
46. Rodgers, M. T.; Armentrout, P. B. A Critical Evaluation of the Experimental and Theoretical Determination of Lithium Cation Affinities. *Int. J. Mass Spectrom.* **2007,** *267*, 167-182.
47. Kesharwani, M. K.; Brauer, B.; Martin, J. M. L. Frequency and Zero-Point Vibrational Energy Scale Factors for Double-Hybrid Density Functionals (and Other Selected Methods): Can Anharmonic Force Fields Be Avoided? *J. Phys. Chem. A* **2014,** *119*, 1701-1714.
48. Beyer, M.; Berg, C.; Joos, S.; Achatz, U.; Hieringer, W.; Niedner-Schatteburg, G.; Bondybey, V. E. The $[Re, O_8]^+$ potential energy surface: fourier transform ion cyclotron resonance collision induced dissociation studies and density functional calculations. *Int. J. Mass Spectrom.* **1999,** *185-187*, 625-638.
49. Lefebvre-Brion, H.; Field, R. W., *The Spectra and Dynamics of Diatomic Molecules*. Elsevier: Amsterdam, 2004.
50. Garcia, M. A.; Morse, M. D. Resonant Two-photon Ionization Spectroscopy of Jet-cooled OsN: 520–418 nm. *J. Chem. Phys.* **2011,** *135*, 114304.
51. Kramida, A.; Ralchenko, Y.; Reader, J.; Team, N. A., NIST Atomic Spectra Database (ver. 5.7.1), [Online]. Available: http://physics.nist.gov/asd. National Institute of Standards and Technology, Gaithersburg, MD.: 2012.
52. Cordero, B.; Gómez, V.; Platero-Prats, A. E.; Revés, M.; Echeverría, J.; Cremades, E.; Barragán, F.; Alvarez, S. Covalent radii revisited. *Dalton Trans.* **2008**, 2832-2838.
53. Rue, C.; Armentrout, P. B.; Kretzschmar, I.; Schröder, D.; Harvey, J. N.; Schwarz, H. Kinetic-energy Dependence of Competitive Spin-allowed and Spin-forbidden Reactions: $V^+ + CS_2$. *J. Chem. Phys.* **1999,** *110*, 7858-7870.
54. Burley, J. D.; Ervin, K. M.; Armentrout, P. B. Translational Energy Dependence of $O^+(^4S) + N_2 \rightarrow NO^+ + N$ from Thermal to 30 eV c.m. *J. Chem. Phys.* **1987,** *86*, 1944-1953.

55. Armentrout, P. B.; Cox, R. M.; Sweeny, B. C.; Ard, S. G.; Shuman, N. S.; Viggiano, A. A. Lanthanides as Catalysts: Guided Ion Beam and Theoretical Studies of Sm^+ + COS. *J. Phys. Chem. A* **2018,** *122*, 737-749.
56. Stowe, G. F.; Schultz, R. H.; Wight, C. A.; Armentrout, P. B. Translational and Electronic Energy Dependence of $S^+ + H_2(D_2,HD) \rightarrow SH^+(SD^+) + H(D)$. Spin-Allowed and Spin-Forbidden Pathways. *Int. J. Mass Spectrom. Ion Processes* **1990,** *100*, 177-195.
57. Ervin, K. M.; Armentrout, P. B. Spin-orbit State-selected Reactions of $Kr^+(^2P_{3/2}$ and $^2P_{1/2})$ with H_2, D_2, and HD from Thermal Energies to 20 eV c.m. *J. Chem. Phys.* **1986,** *85*, 6380-6395.
58. Ervin, K. M.; Armentrout, P. B. Spin Orbit State selected Reactions of $Xe^+(^2P_{3/2}$ and $^2P_{1/2})$ with H_2, D_2, and HD. *J. Chem. Phys.* **1989,** *90*, 118-126.
59. Person, W. B.; Zerbi, G., *Vibrational Intensities in Infrared and Raman Spectroscopy*. Elsevier Scientific Pub. Co.: 1982.
60. Herzberg, G., *Molecular Spectra and Molecular Structure*. Van Nostrand Reinhold: New York, 1966; Vol. III.
61. Irikura, K. K. Experimental Vibrational Zero-Point Energies: Diatomic Molecules. *J. Phys. Chem. Ref. Data* **2007,** *36*, 389-397.

Table 1. Molecular parameters for the PST competitive model

Species	Vibrational Frequencies (ω_e; cm^{-1}) [a]	Rotational Constants (B, cm^{-1}) [a]	Number of accessible surfaces	E_0 (eV) [b]
$Re^+ + SO_2$	513, 1163, 1360	1.989, 0.343, 0.292	7	0.0
$ReO^+ + SO$	1157, 1145	0.440 (2) , 0.713 (2)	6	1.00 ± 0.04
$ReO_2^+ + S$	1074, 994, 348	0.710, 0.275, 0.198	7	0.28 ± 0.02
$ReSO^+ + O$	1027, 560, 276	0.534, 0.125, 0.102	2	1.13 ± 0.11

[a] Degeneracies in parentheses. Values are calculated at the B3LYP/def2-TZVPPD level of theory. For comparison, experimental values for SO_2 are ω_e = 518, 1151, 1362 cm^{-1} and B = 2.027, 0.344, 0.294 cm^{-1} and for SO are ω_e = 1151 cm^{-1} and B = 0.721(2) cm^{-1}.[5, 59-61]

[b] Threshold energy to form products from the reactants, $Re^+ + SO_2$.

Table 2. Parameters for modeling with eq (1) and the dissociation energy [a]

Species	Energy Range (eV)	σ_0	n	E_0 (eV)	p	E_D (eV)
ReO^+	0 – 2.2	9.7 ± 1.1	2.2 ± 0.1	0.88 ± 0.05		
ReO_2^+	0 – 2.2	5.9 ± 0.4	2.2 ± 0.1	0.15 ± 0.02		
$ReSO^+$	0 – 8	0.6 ± 0.1	1.7 ± 0.1	1.31 ± 0.12	5	6.03 ± 0.08

[a] Uncertainties are one standard deviation.

Table 3. Experimental (current and literature GIB studies) and theoretical bond dissociation energies (eV) of the products

Species	Experimental [a]				Theoretical [b]
	$M^+ + SO_2$ MLOC	$M^+ + O_2$ GIB Study [c, d]	$M^+ + CO$ GIB Study [e]	Literature	B3LYP/def2-TZVPPD
Re^+-O	4.78 ± 0.06	4.82 ± 0.03	4.67 ± 0.09	5.0 ± 1.3 [f]	4.70 ($^3\Delta_3$) [d]
					4.57 ($^5\Pi_{-1}$) [d]
Re^+-O_2	5.75 ± 0.02			7.1 ± 2.3 [g]	5.00 ($^3B_1$) [d]
Re^+-S					3.67 ($^5\Pi_{-1}$)
ORe^+-O	6.05 ± 0.05			7.5 ± 3.6 [h]	5.53 ($^3B_1$) [d]
Re^+-SO	4.35 ± 0.14				3.74 (^{3}A")
ORe^+-S	4.89 ± 0.19				4.44 (^{3}A")

[a] Uncertainties are one standard deviation. [b] S.O. corrected. See text. [c] Also serves as the weighted average of all GIB values. [d] Reference [1]. [e] Reference [4]. [f] Reference [48]. [g] References [1, 48]. [h] References [1, 5, 48].

Table 4. Theoretical calculations at various levels of theory for ReS^+

State	Level	Basis Set	r(M-S) (Å)	E (E_h)	ω_e (cm^{-1}) [a]	D_0/E_{rel} (eV)	D_0/E_{rel} (eV) [b] incl S.O.
$^5\Pi$	B3LYP	def2-TZVPPD	2.087	-476.175726	505	3.52	3.67
		aug-cc-pV5Z	2.079	-476.490347	510	3.57	3.73
	BP86	aug-cc-pV5Z	2.076	-476.611406	548	4.16	4.32
	CCSD(T) [c]	def2-QZVPPD	2.085	-475.470883	509	3.17	3.33
		CBS(aug-cc-pVXZ)[d]		-475.891214	525	3.42	3.58
$^3\Sigma^-$	B3LYP	def2-TZVPPD	2.010	-476.162277	587	*0.37*	*0.52*
		aug-cc-pV5Z	2.003	-476.477356	592	*0.35*	*0.51*
	BP86	aug-cc-pV5Z	2.006	-476.596503	615	*0.41*	*0.56*
	CCSD(T) [c]	def2-QZVPPD	2.009	-475.455045	590	*0.43*	*0.59*
		CBS(aug-cc-pVXZ)[d]		-475.877636	577	*0.37*	*0.53*
$^3\Delta$	B3LYP	def2-TZVPPD	2.014	-476.154834	602	*0.57*	*0.41*
		aug-cc-pV5Z	2.007	-476.469408	606	*0.57*	*0.41*
	BP86	aug-cc-pV5Z	2.012	-476.591087	618	*0.55*	*0.40*
	CCSD(T) [c]	def2-QZVPPD	2.013	-475.445125	593	*0.70*	*0.54*
		CBS(aug-cc-pVXZ)[d]		-475.867933	596	*0.63*	*0.48*

[a] Vibrational frequencies scaled by factors indicated in Table S1 (ESI†). [b] Bond dissociation energy (roman) or energy relative to ground state (italic). [c] CCSD(T) single point calculations are performed using B3LYP optimized geometries and zero point energy corections. [d] Complete basis set limit obtained as discussed in the text.

Table 5. Various states of $ReSO^+$ calculated at B3LYP/def2-TZVPPD

Molecules	State	r(Re-S) (Å)	r(Re-O) (Å)	r(S-O) (Å)	∠SReO	E (E_h)	ω_e (cm^{-1}) [a]	E_{rel} [b]
$OReS^+$	$^3A''$	2.077	1.667		111.1	-551.479630	276, 560, 1027	0.00
$OReS^+$	$^1A'$	2.050	1.648		104.0	-551.472776	320, 582, 1077	0.19
$OReS^+$	$^5A''$	2.260	1.663		126.6	-551.431801	161, 398, 1038	1.30
$ReOS^+$	$^5A'$	2.232	1.889	1.688	47.5	-551.405990	393, 548, 790	2.00
$ReOS^+$	$^3A''$	2.184	1.984	1.594	44.6	-551.386614	322, 415, 893	2.53
$ReOS^+$	$^7A''$	2.685	1.928	1.618	36.6	-551.381659	185, 601, 797	2.67
$ReSO^+$	$^3\Sigma^-$	1.969		1.432	0.0	-551.376883	103(2), 467, 1337	2.80
$ReOS^+$	$^3\Sigma^-$		1.822	1.531	0.0	-551.368879	183(2), 378, 1047	3.01
$OReS^+$	$^7A''$	2.673	1.693		130.4	-551.359306	101, 201, 992	3.27
$ReOS^+$	$^1A'$	2.110	1.876	1.682	49.5	-551.358451	411, 530, 819	3.30
$ReSO^+$	$^1\Gamma$	1.951		1.428	0.0	-551.339076	177(2), 512, 1365	3.82
$ReOS^+$	$^1\Gamma$		1.730	1.551	0.0	-551.308946	258(2), 459, 1137	4.64

[a] Vibrational frequencies scaled by 0.9885, see Table S1 (ESI†).

[b] Energy relative to ground state $OReS^+$ ($^3A''$).

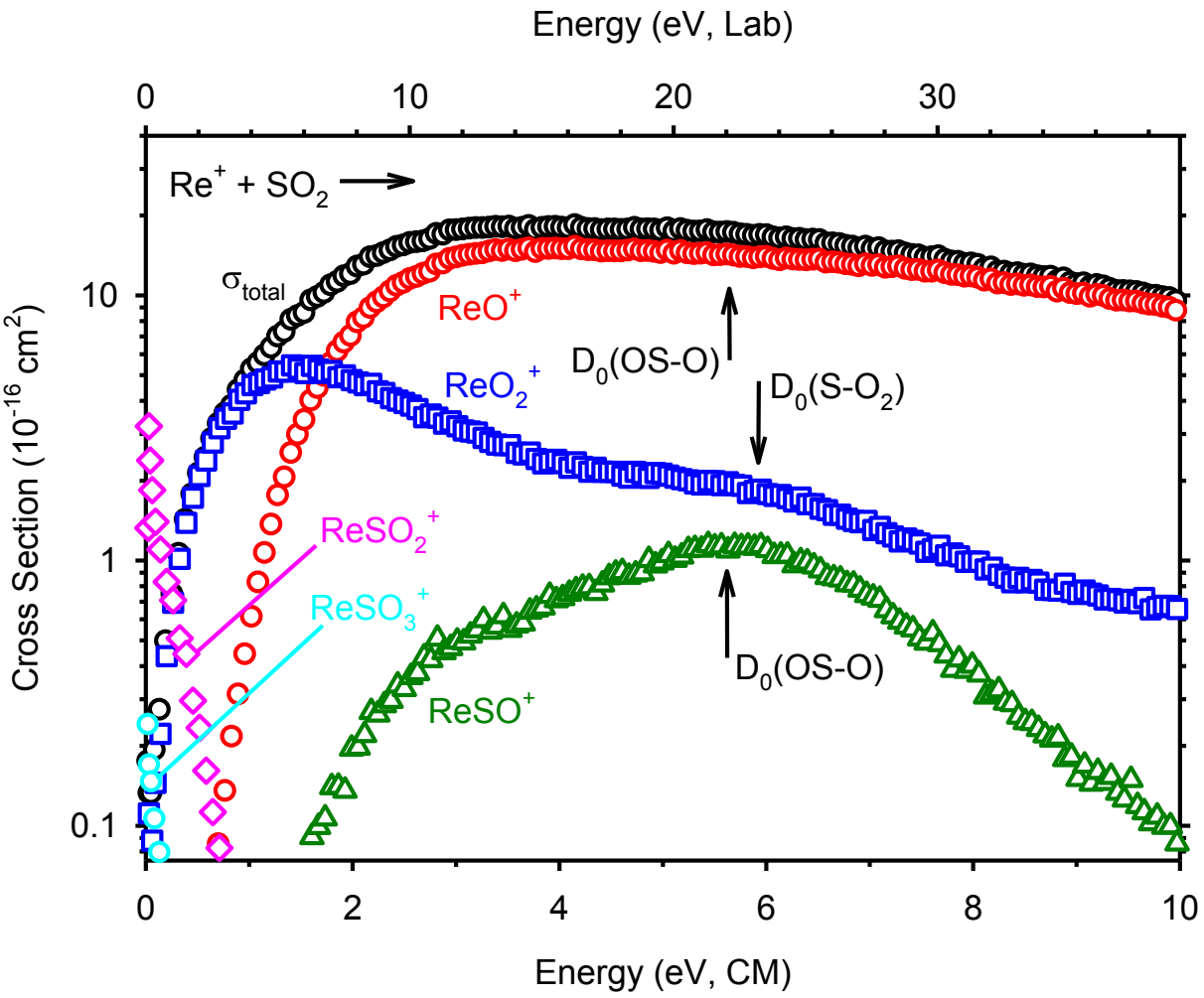

Fig. 1 Cross sections (taken at 0.3 mTorr SO_2 pressure) for the reaction of $Re^+ + SO_2$ as a function of center-of-mass frame (lower axis) and laboratory frame (upper axis) energies to form ReO^+ (red circles), ReO_2^+ (blue squares), $ReSO^+$ (green triangles), $ReSO_2^+$ (pink diamonds), and $ReSO_3^+$ (cyan circles). Black circles represent the sum of all product cross sections excluding $ReSO_2^+$ and $ReSO_3^+$. Vertical arrows indicate D_0(O-SO) = 5.66 eV and D_0(S-O_2) = 5.90 eV.[5]

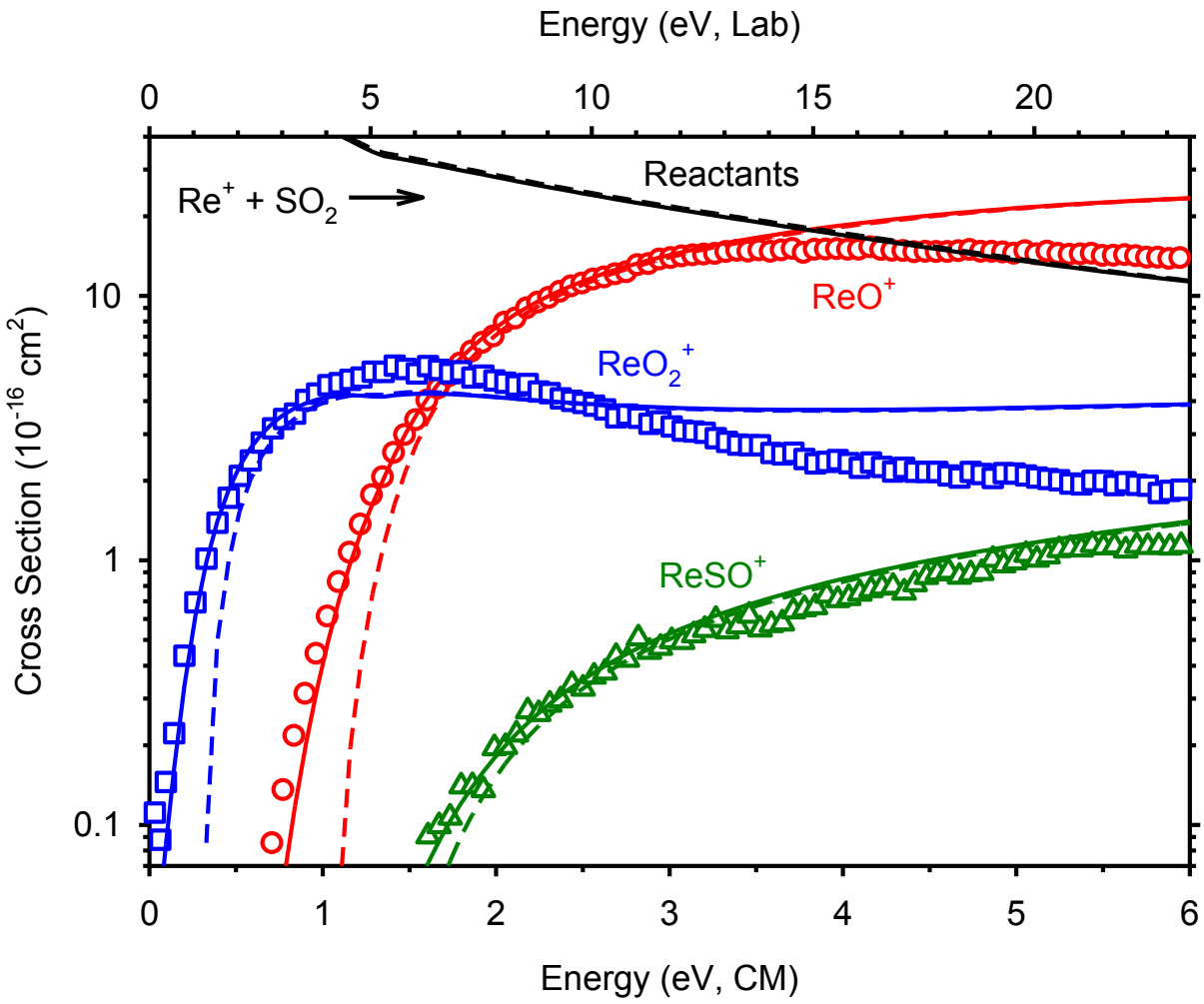

Fig. 2 Pressure-independent cross sections (symbols) for reactions of $Re^+ + SO_2$ as a function of the center-of-mass frame (lower axis) and laboratory frame (upper axis) energy. Solid lines represent the phase space theory model cross sections convoluted over the reactant internal and kinetic energy distributions and include the return to reactants (black line). The dashed lines are the models in the absence of internal and kinetic energy distributions for reactants at 0 K.

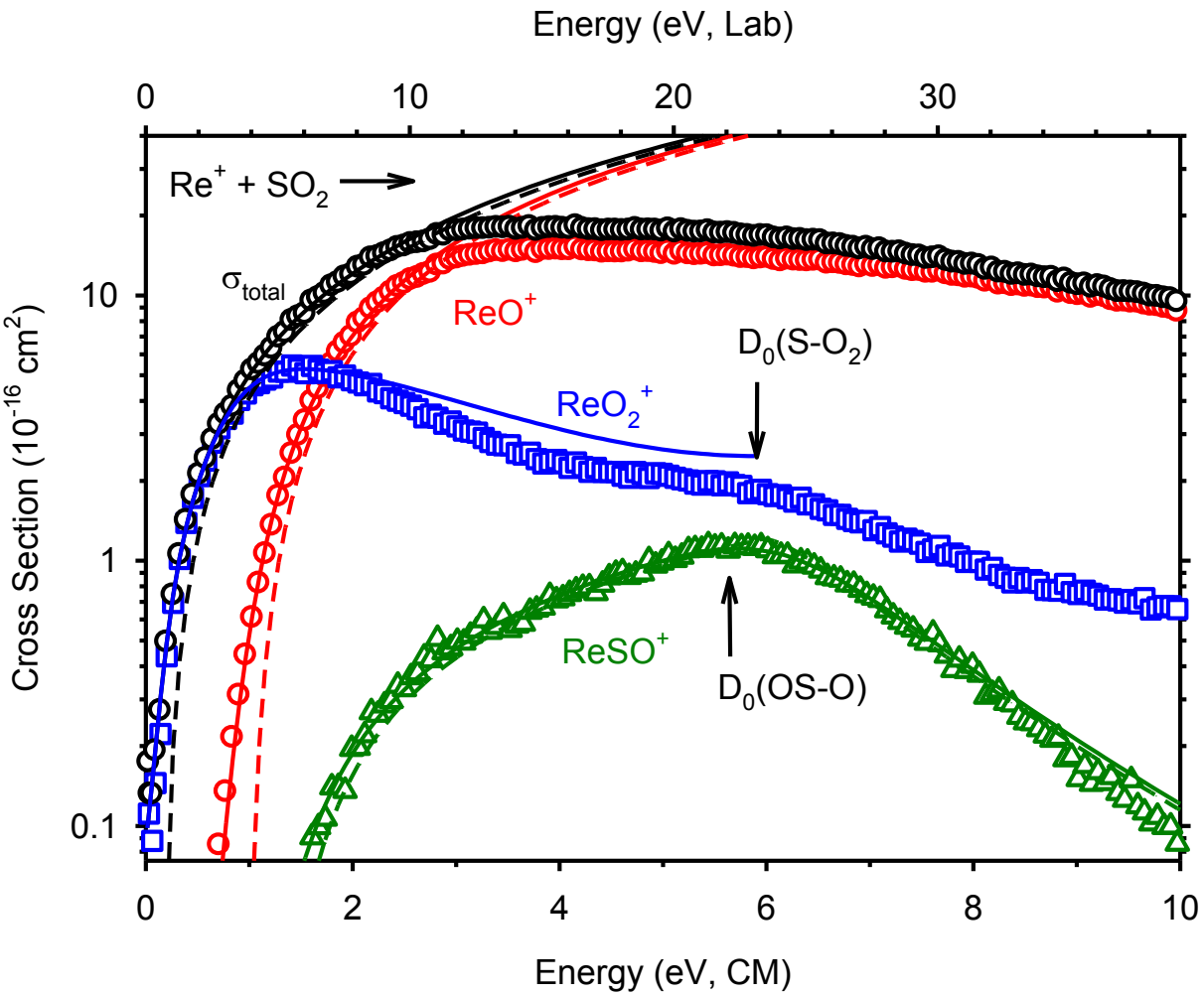

Fig. 3 Pressure-independent cross sections (symbols) for reactions of $Re^+ + SO_2$ as a function of the center-of-mass frame (lower axis) and laboratory frame (upper axis) energy to form ReO^+ (red circles), ReO_2^+ (blue squares), $ReSO^+$ (dark green triangles), and total (black circles). Red and black solid lines represent the model cross sections of eq (1) convoluted over the reactant internal and kinetic energy distributions. The blue line shows the difference between the red and black models. Dashed lines are the models in the absence of kinetic energy distributions for reactants at 0 K. Vertical arrows indicate D_0(O-SO) = 5.66 eV and D_0(S-O_2) = 5.90 eV.[5]

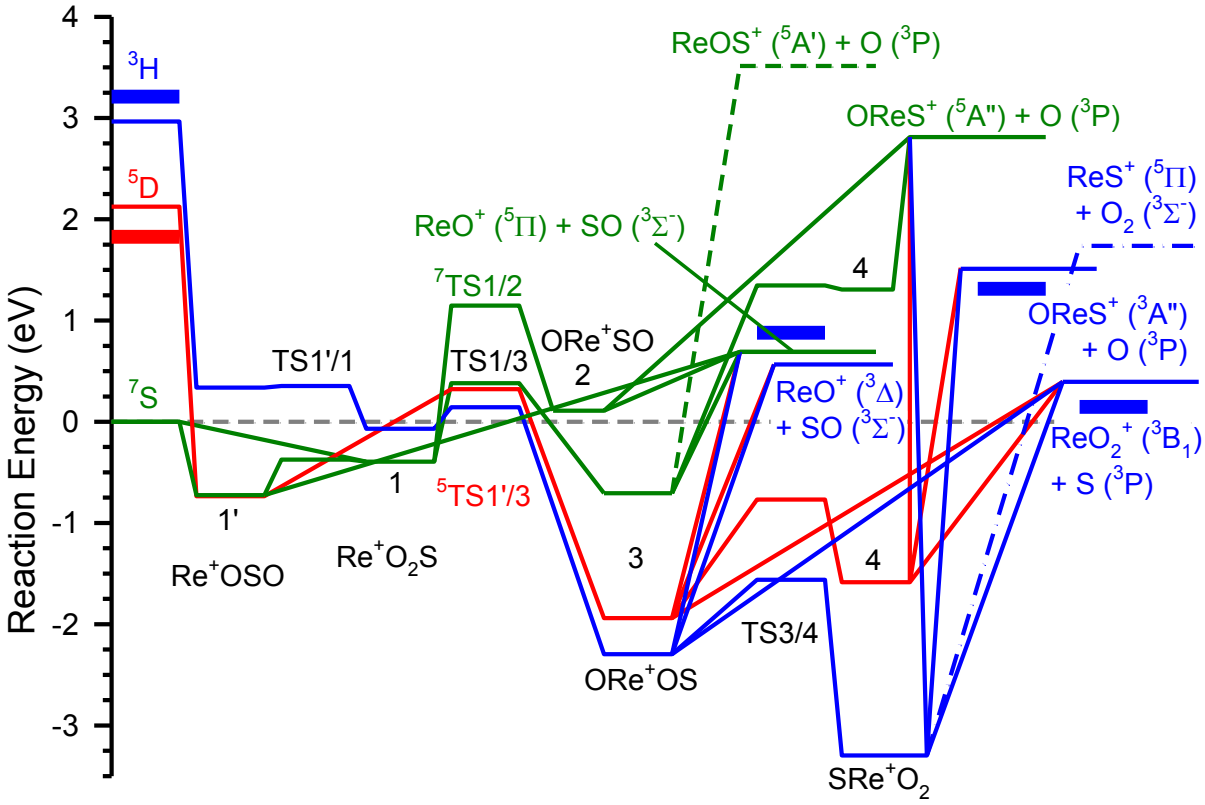

Fig. 4 Potential energy surface (without S.O. correction) for the reaction $Re^+ + SO_2$ calculated at the B3LYP/def2-TZVPPD level relative to the ground state reactant energy. The thick horizontal lines represent the experimental energies of the reactants and products relative to ground state reactants. The thin horizontal lines represent the theoretical energies for septet (green), quintet (red), and triplet (blue) surfaces. Structures of all intermediates and transition states are shown in Figure 5.

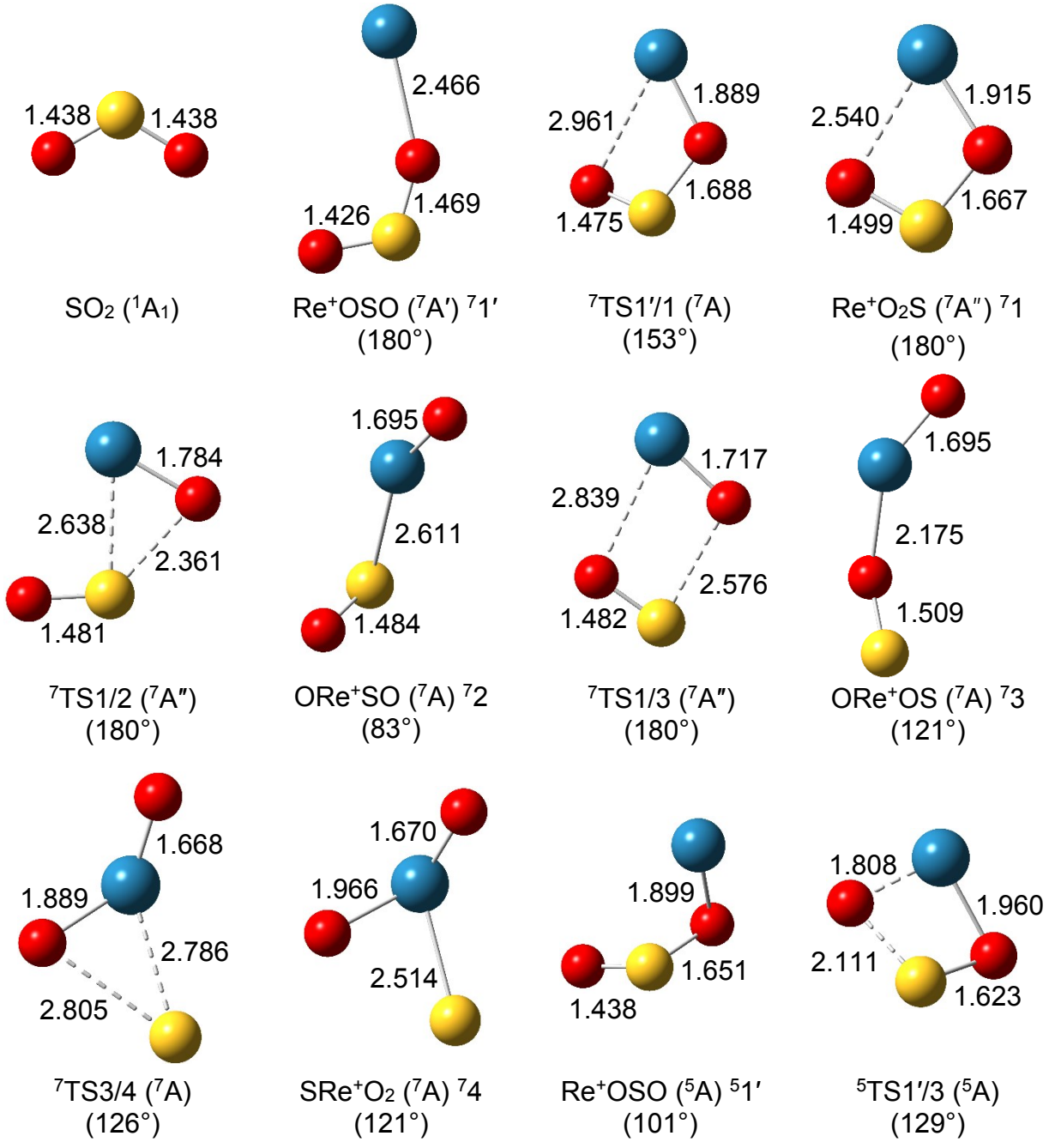

Fig. 5 Geometrical structures of SO_2 reactant and $ReSO_2^+$ intermediates in Figure 4. These structures are optimized at the B3LYP/def2-TZVPPD level with bond lengths indicated in Å. The value in parenthesis is the dihedral angle (∠OReSO).

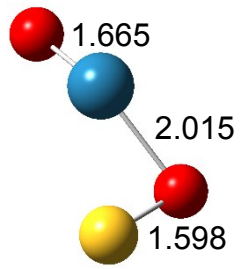

ORe^{+}OS (^{5}A) ^{5}3
(111°)

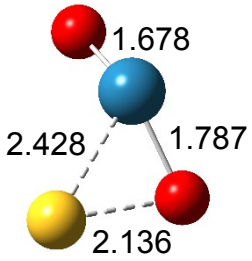

^{5}TS3/4 (^{5}A)
(125°)

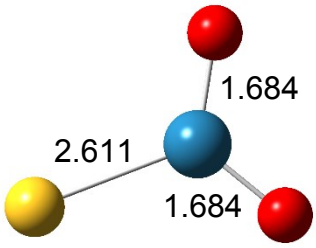

SRe^{+}O$_2$ (^{5}B$_2$) ^{5}4
(180°)

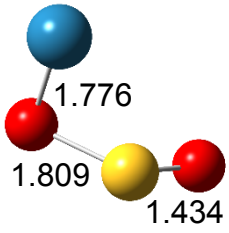

Re^{+}OSO (^{3}A) ^{3}1′
(100°)

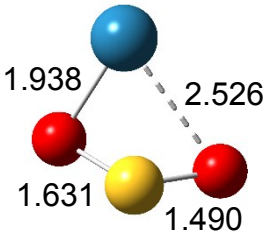

^{3}TS1′/1 (^{3}A)
(115°)

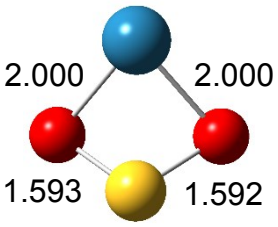

Re^{+}O$_2$S (^{3}A″) ^{3}1
(121°)

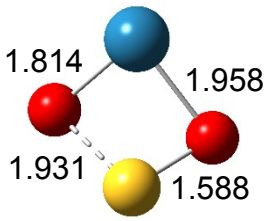

^{3}TS1/3 (^{3}A)
(124°)

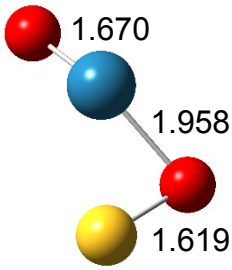

ORe^{+}OS (^{3}A) ^{3}3
(113°)

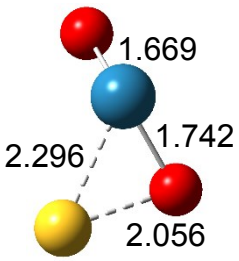

^{3}TS3/4 (^{3}A)
(105°)

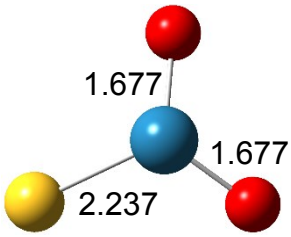

SRe^{+}O$_2$ (^{3}A″) ^{3}4
(131°)

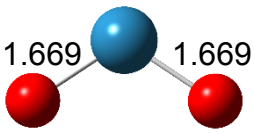

ReO$_2^{+}$ (^{3}B$_1$)

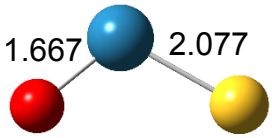

OReS^{+} (^{3}A″)

Fig. 5 Continued

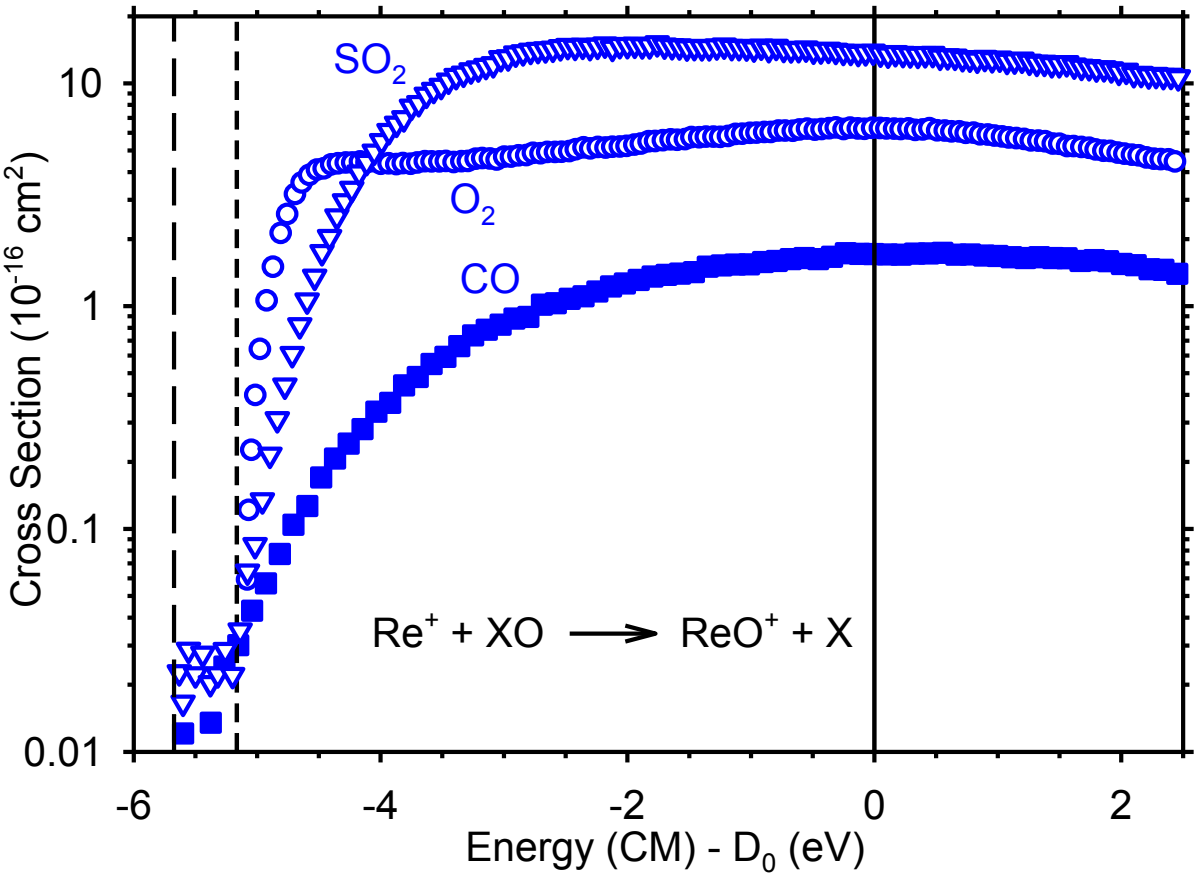

Fig. 6 Cross sections for the reactions of SO_2 (inverted triangles), O_2 (circles), and CO (squares) with Re^+scales as a function of the center-of-mass frame energy minus the BDE of the neutral reactant, D_0(O-SO) = 5.66 eV, $D_0(O_2)$ = 5.12 eV, and D_0(CO) = 11.11 eV.[5] Vertical lines indicate the zero of energy for the SO_2 (long dash) and O_2 (short dash) systems, and the 0 K BDE of the neutral reactant (solid) at 0 eV.